J Mater Sci (2010) 45:6498–6504
DOI 10.1007/s10853-010-4738-3

Investigation of microstructural characteristics of nanocrystalline 12YWT steel during milling and subsequent annealing by X-ray diffraction line profile analysis

R. Rahmanifard · H. Farhangi · A. J. Novinrooz · N. Afshari

Received: 21 February 2010 / Accepted: 25 June 2010 / Published online: 9 July 2010

Abstract The variations of dislocation density, character of dislocations, and crystallite size as a function of milling time and post-heat-treating temperature were investigated for 12YWT nanocomposite ODS ferritic steel using X-ray diffraction line profile analysis. The modified Williamson–Hall and the modified Warren–Averbach methods, which are based on the dislocation model of the strain anisotropy, were utilized to characterize the microstructural parameters of the nanocomposite material and the matrix alloy. The presence of nano-oxide particles in the ODS steel caused an initially sharp decrease in the average crystallite size; however, with increasing milling time, the crystallite size of the unreinforced alloy reached the comparable value of that of the reinforced material. The subsequent heat treating on the powders milled for 80 h showed that the presence of Y_2O_3 dispersoids increased the recrystallization temperature and suppressed the grain growth up to 800 °C in the 12YWT alloy as compared to the matrix alloy which occurred about 700 °C. The results of X-ray diffraction line profile analysis also showed that the contribution of edge components of the dislocations increased at the initial milling stages, while the screw components tended to increase after 40-h milling time.

R. Rahmanifard (✉) · H. Farhangi
School of Metallurgy and Materials Engineering, College of Engineering, University of Tehran, Tehran, Iran
e-mail: rahmanifrd@ut.ac.ir

R. Rahmanifard · A. J. Novinrooz · N. Afshari
Advanced Materials Group, School of Materials Research, P.O. Box 31585-4395, Karaj, Iran

Introduction

The nanocomposite oxide dispersion strengthened (ODS) ferritic steels exhibit superior creep and tensile properties as well as superior void swelling resistance at high temperatures, and hence, these materials have been considered as a suitable choice for fuel cladding [1–3]. The most commonly used route to produce ODS steels is mechanical alloying (MA), in which a mixture of metal or alloy powders and oxide powder is milled for a long period of time in a high-energy ball mill. The milling process heavily deforms the alloying powders and introduces a variety of crystal defects such as dislocations, vacancies, stacking faults, and increased number of grain boundaries into the powder particles, which lead to increased lattice strains and refining of crystalline domains [4]. These parameters can influence the subsequent treating conditions of the mechanically alloyed powders by altering their transformation behavior, phase constitution, or distribution of the particles formed after the secondary thermal treating [4–6]. Thermal studies on the mechanically alloyed powders of ODS Steels have revealed that the reduction of alloyed powder grain size during milling to the nanometer range increases the locations susceptible to the precipitating of oxide nano-clusters during annealing resulting in improved distribution of oxide particles and retention of sub-micron grain size at high temperature consistent with those in the as-milled powders which can result in improved mechanical properties [6].

X-ray diffraction line broadening analysis is an authoritative method to determine the microstructural characteristics of ultrafine-structured materials. The effects of crystallite size and lattice strain on peak broadening can be separated on the basis of diffraction order independence and dependence, respectively [7, 8]. However, in metal

alloys, the anisotropic strain field of dislocations results in non-monotonic order dependence of the strain broadening of diffraction peaks. The modified Williamson–Hall and modified Warren–Averbach methods unlike their classical methods take into account the strain anisotropy using the contrast factor of dislocation and also provide additional microstructural characterization consisting of the average crystalline size, log-normal size distribution, and dislocation structure [9].It has been reported that the dislocation structure and subgrain-size distribution in fatigued MANET steel obtained by aforementioned methods indicate a good agreement between X-ray line broadening results and transmission electron microscopy (TEM) observations [10]. X-ray diffraction study on a nanostructured 18Ni maraging steel also shows that the measured mean grain size corresponds reasonably with the dislocation cell size observed by means of TEM [11]. Schafler [12] and Ungar [13] have also reported that the measured densities of screw and edge dislocations during the deformation by means of X-ray line profile analysis are in agreement with those of the existing deformation models.

In this study, the effects of milling time and subsequent annealing temperature on the microstructural properties of nanocomposite ODS steel were investigated using X-ray diffraction peak profile analysis and compared with those of unreinforced alloy to specify the role of particles.

Experimental procedure

Specimen preparation

The 12YWT–ODS steel with the chemical composition of Fe–12.3Cr–3.0W–0.4Ti–0.25Y_2O_3 (in weight percentage) was prepared by mechanical alloying, using high-purity metal powders of Fe–Cr, W, Ti, and Y_2O_3 particles sized between 20 and 30 nm (Merck & Aldrich Companies). The powder mixture was mechanically blended for 2 h before milling. The mechanical alloying was performed in a high-purity Ar (99.9999 wt%) atmosphere for 4, 8, 12, 20, 30, 40, 50, and 80 h with the rotation speed of 420 rpm and the ball-to-powder weight ratio of 10:1 using a water-cooled vertical high-energy attrition mill (Union Process 1-S). Since both, the balls and the jar of the mill, were made of chromium hardened steel, there was no metal contamination in the products. In order to understand the thermal stability of the microstructure of the mechanically alloyed powder, the 80-h milled powders were annealed at 700, 800, and 900 °C under vacuum of 10^{-4} mbar for 1 h.

In order to investigate the microstructural characteristics of the specimens, X-ray diffraction analyses were performed by a Philips Analytical X-ray diffractometer PW1800 using Cu Kα ($\lambda = 0.15406$ nm) radiation. Step size and step time were 0.02 and 2 s per step, respectively. The instrumental pattern was measured on a well-annealed Fe powder. For accurate calculation of peak breadth, the background removal and Cu Kα_2 stripping were carried out by the MKDAT software program.

Evaluation of X-ray diffraction profile

In order to calculate the microstructural parameters from the diffraction profiles, the Williamson–Hall and Warren–Averbach methods were employed. The Williamson–Hall method is based on full widths at half maximum (FWHM) or integral breadth of the experimental peak profile, which is presented as $\Delta K = \cos\theta(\Delta 2\theta)/\lambda$. As mentioned before, the peak broadening is due to size and strain variations; hence FWHM is written as follows [7, 8]:

$$\Delta K = \Delta K^{s} + \Delta K^{d} \tag{1}$$

where ΔK^{s} and ΔK^{d} are affected by grain size and lattice distortion, respectively. $K = 2\sin\theta/\lambda$ is defined as the diffraction vector, θ is the diffraction angle, and λ is the wavelength of X-ray. According to the classical Williamson–Hall method, $\Delta K^{s} = \gamma/D$, where $\gamma = 0.9$ for the FWHM, and $\gamma = 1$ for the integral breadth and D is the volume-weighted grain size, and $\Delta K^{d} = A\varepsilon K$, where A is a constant depending on strain distribution. By plotting the values of ΔK as a linear function of K, the volume crystallite size and lattice strain can be obtained. Assuming that the strain broadening is caused by the dislocations in the modified Williamson–Hall method, ΔK^{s} is the same term of the classical method but ΔK^{d} will be according to [14]:

$$\Delta K^{d} = \frac{\pi M^2 b^2}{2}\rho^{\frac{1}{2}}\left(K^2\bar{C}\right) + O\left(K^2\bar{C}\right)^2 \tag{2}$$

where ρ and b are the average dislocation density and the length of the Burgers vector of dislocations, respectively. M is a constant depending on the effective outer cut-off radius of dislocations, $\bar{C}$ are the average contrast factors of dislocations depending on the relative positions of the diffraction vector and also the Burgers and line vectors of the dislocation, and O stands for higher order terms in $K^2\bar{C}$ and has a relatively small value. It can be shown that the average dislocation contrast factors in an untextured cubic polycrystalline material are a simple function of the invariants of the fourth order polynomials of the Miller indices (hkl) as follows [14]:

$$\bar{C} = \bar{C}_{h00}\left(1 - qH^2\right) \tag{3}$$

where $\bar{C}_{h00}$ is the average dislocation contrast factor for the $h00$ reflections, q is a parameter depending on the elastic constants of the crystal and the edge, or screw character of dislocations, and H^2 is a constant for a (hkl) Bragg

reflection, which is expressed as $H^2 = (h^2k^2 + h^2l^2 + k^2l^2)/(h^2 + k^2 + l^2)^2$. The experimental values of q also provide information about the screw, the edge, or the mixed character of dislocations as compared with the theoretical values. The values of q and D are obtained by the linear least squares method from Eq. 1 considering ΔK^{s} and ΔK^{d} in the modified relationship.The modified Warren–Averbach equation was also utilized to obtain dislocation density [14]:

$$LnA(L) = LnA^{S}(L) - \frac{\rho\pi b^2}{2}L^2 \ln\left(\frac{R_e}{L}\right)\left(K^2\bar{C}\right) + O\left(K^2\bar{C}\right)^2 \quad (4)$$

where $A(L)$ are the absolute values of the Fourier coefficients of the diffraction profiles, $A^{S}(L)$ are the size Fourier coefficients, R_e is the effective outer cut-off radius of dislocations, and O is a small value, which stands for higher-order terms in $K^2\bar{C}$. L is the Fourier length defined as $L = na_3$, where $a_3 = \lambda/2(\sin\theta_2 - \sin\theta_1)$, n are the integers starting from zero, and $(\theta_2 - \theta_1)$ is the angular range of the measured diffraction peak profile. The dislocation density can be calculated by plotting the coefficient of the second term in Eq. 4 as a linear function of $Ln(L)$. The intersection of the initial slope of the size Fourier coefficients curve at $A^{S}(L) = 0$ yields the area-weighted average column length, L_0. By calculating the size parameters of D, d, and L_0 from FWHM, integral breadth, and Fourier coefficients, respectively, log-normal size distribution factor, which is confirmed for grain size distribution in the milling procedure [15], can be determined by following equation [16]:

$$f(x) = \frac{1}{\sqrt{2\pi}}\frac{1}{\sigma x}\exp\left[-\frac{\left(\ln\left(\frac{x}{m}\right)\right)^2}{2\sigma^2}\right] \quad (5)$$

where x is a crystallite size, m and σ are the parameters of distribution. m is the median, and σ is the variance of the normal distribution function that for spherical crystallites are proportional to the volume and area-weighted average crystallite sizes:

$$\langle x\rangle_{vol} = \frac{4}{3}d = m\exp\left(3.5\sigma^2\right) \quad (6)$$

$$\langle x\rangle_{area} = \frac{3}{2}L_0 = m\exp\left(2.5\sigma^2\right) \quad (7)$$

Results and discussion

Mechanical alloying

Figure 1 shows the X-ray diffraction patterns of the mechanically alloyed 12YWT-ODS ferritic steel powders for different milling times. These patterns are characterized by four main peaks of (110), (200), (211), and (220) referring to α-Fe, and the other five peaks of (110), (200), (211), (220), and (310) indicating unalloyed B.C.C tungsten phase that resolves within the structure with further milling. As shown in Fig. 1, with increasing milling time, the peak broadening is enlarged. The FWHM values of Bragg reflections are shown in Fig. 2 as a function of K for various milling times according to the conventional Williamson–Hall plot. It can be seen that line broadening does not increase with the order of reflections monotonously and deviation from the linear regression intensifies with increasing milling time. This is indicative of the strain anisotropy induced by dislocations, which is taken into account by the average contrast factors of dislocations. Assuming the elastic constants of α-Fe as $c_{11} = 237$ GPa, $c_{12} = 141$ GPa, and $c_{44} = 116$ GPa, the average values of dislocation contrast factor for edge and screw dislocations are calculated with the Burgers vector $a/2\langle 111\rangle$ for $\langle 111\rangle\{110\}$, and $\langle 111\rangle\{211\}$ slip systems. The calculated values of the average contrast factor of the pure screw and pure edge dislocations for all the reflections are listed in Table 1. The value of $\bar{C}_{h00}$ is determined by assuming that

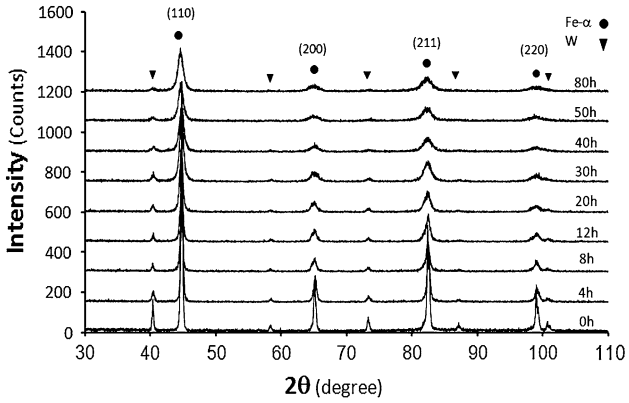

Fig. 1 The X-ray diffraction patterns for different milling times

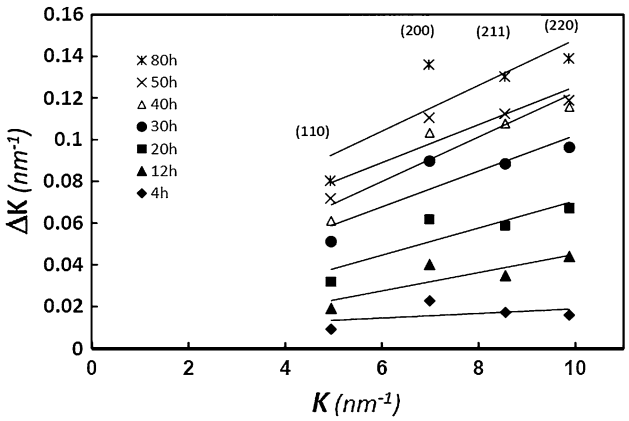

Fig. 2 The classical Williamson–Hall plot for different milling times

Table 1 The calculated values of the average contrast factor of pure edge and pure screw dislocations for the different reflections

Reflection	$\bar{C}_{hkl}^{edge}$	$\bar{C}_{hkl}^{screw}$	$\frac{1}{2}\bar{C}_{hkl}^{edge} + \frac{1}{2}\bar{C}_{hkl}^{screw}$
110	0.179117	0.104	0.141558
200	0.2424	0.3042	0.2733
211	0.179121	0.103975	0.141548
220	0.179117	0.104	0.141558

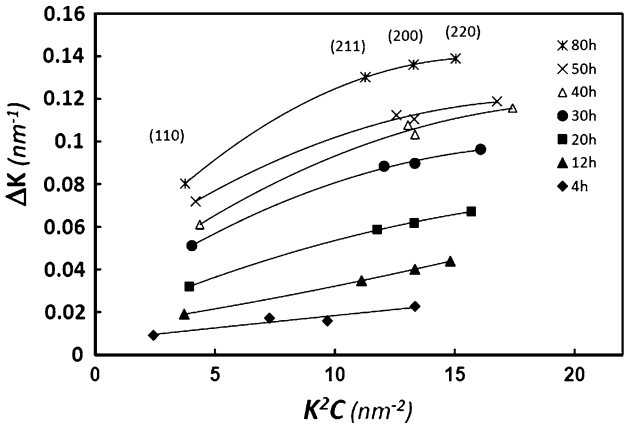

Fig. 3 The modified Williamson–Hall plot for different milling times

the edge and screw dislocations are present with equal proportions in the crystal structure (Table 1).Subsequently, utilizing the experimental q values from Eq. 3, the average contrast factors are determined. Theoretical values of the character of dislocation for pure screw (q_{screw}) and pure edge (q_{edge}) dislocations are obtained by means of Eq. 3 as 2.632 and 1.044, respectively. Figure 3 shows the FWHM values as modified Williamson–Hall plot at $K^2\bar{C}$ scale. It is observed that the data are well fitted in a quadratic regression procedure indicating the authenticity of the dislocation model. Since no strain broadening is present at $K = 0$, the corresponding ΔK value is due only to size broadening, by extrapolating from the measured data points at $K = 0$, the volume-weighted crystallite size can be found based on the FWHM or the integral breadth. The average volume crystallite size measurements for the composite and the matrix material with different milling times are shown in Fig. 4. At the initial stages of milling, the crystalline domain size decreases rapidly and after only 8 h of milling, it reaches 55 nm. Similar trends have been reported in the literature [6]. As seen, the presence of oxide particles in the composite material causes an initially sharp slope as compared with the unreinforced alloy. However, with increasing milling time, the average crystallite size of the unreinforced alloy approaches the same value observed for the composite material, which is in about 20 nm at 80 h of milling. It is known that crystallite size is related to the

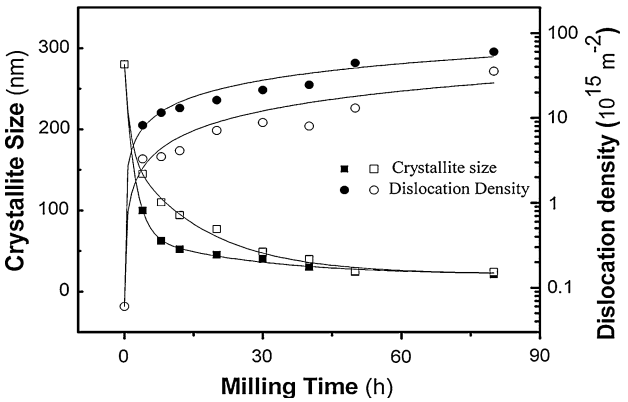

Fig. 4 Variations of average crystallite size and dislocation density with milling time for the composite material (*solid*) and the matrix alloy (*open*)

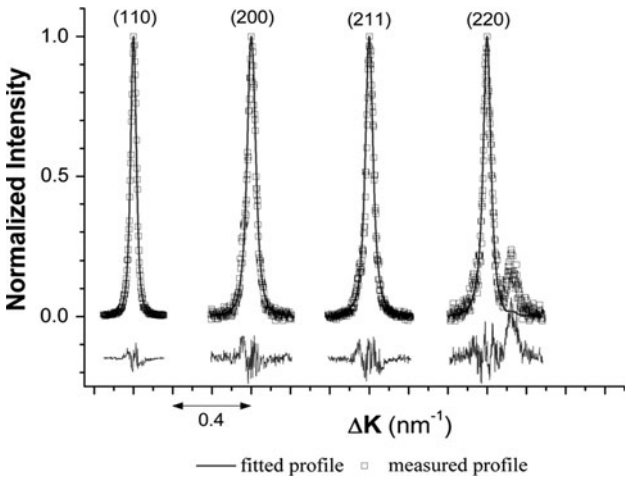

Fig. 5 The measured and the theoretically fitted intensity profiles versus diffraction vectors of ODS-steel milled for 4 h. The difference plot between the measured and the fitted profiles is also shown in lower part of figure. The scale of the differences is the same as in the main part of the figure

density of dislocation defects [17]. In order to calculate the dislocation density according to Eq. 4, Fourier transform of diffraction pattern is utilized. Since a correct Fourier analysis is very sensitive to the quality of data, all of the peaks are fitted by Voigt function through the MKDAT software, and the resulting data are used to determine the Fourier coefficients. The typical measured and theoretical fitted intensity profiles are plotted in Fig. 5. The difference plot between the measured and the fitted patterns is also given at the bottom of the figure. As observed, a relatively good quality of the fitting has been obtained. The absolute values of the Fourier coefficients are plotted according to the modified Warren–Averbach method as shown in Fig. 6 for different Fourier lengths. By interpolating the smooth quadratic curve through the measured data, the dislocation density is attained, which is plotted as a function of milling

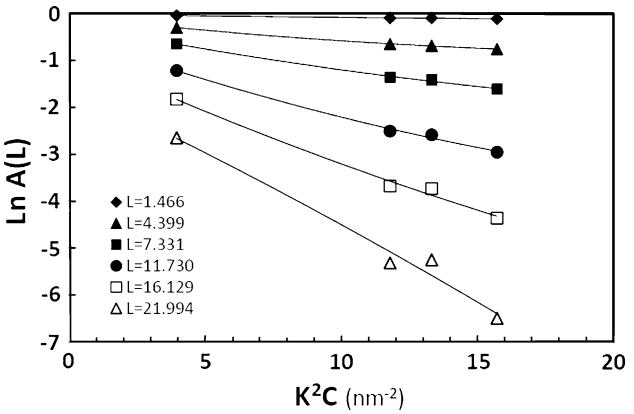

Fig. 6 The modified Warren–Averbach plot for different fourier length of specimen milled for 20 h

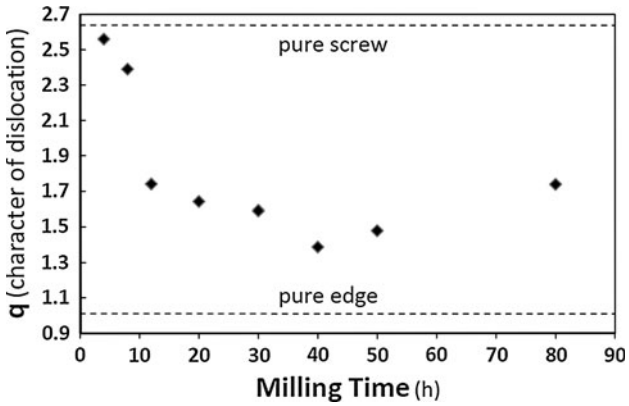

Fig. 7 The variation of character of dislocation with milling time

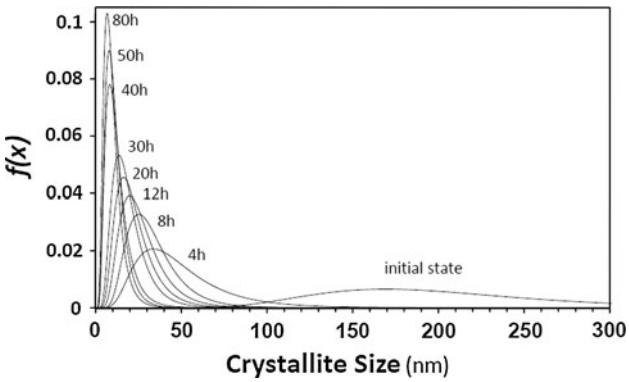

Fig. 8 The log-normal size distribution function, $f(x)$, for different milling times of ODS-steel

time in Fig. 4. At the initial milling stages, the average dislocation density increases at a significant rate, but it diminishes at higher milling times. The rate of increase in dislocation density is notably enhanced by the presence of nano-oxide particles in the reinforced steel.

Owing to the heavy deformations induced by different types of collisions during the initial milling stages, complex dislocation arrays are generated, which lead to accumulation of dislocations and a sharp increase in dislocation density (Fig. 4). At higher deformations, the preferred rearrangement of the cell structured dislocations induced by annihilation of dislocations during the milling process results in refined crystallite size and reduction in the rate of rise of dislocation density. More rapid decrease of the crystallite size at the initial milling stages observed in the reinforced material can be attributed to the role of particles in dislocation pile up formation as well as the influence of particle interspacing on crystallite size. The annihilation event mainly occurs through cross slipping of the screw components during the cold deformations according to the plastic deformation mechanisms [18, 19]. The reduced proportion of the screw components of dislocations with increasing milling time is clearly shown in Fig. 7, where the character of dislocation is plotted as a function of milling time. It is observed that with increasing milling time, the contribution of screw components is reduced. However, a slight increase in the screw components is noted after 40 h milling. It can also be seen in Fig. 4 that while the crystallite size shows no notable change at higher milling times, the dislocation density continues to rise with milling. According to the theorem proposed by Fecht [17], for high-energy ball milling, the severe deformations during the milling may lead to disintegration of the original grains when some low-angle boundaries are rearranged into high-angle boundaries as a result of grain boundary rotation. Hence, the newly generated dislocations can migrate to these new incoherent boundaries resulting in increased dislocation density as well as screw components of dislocations. Figure 8 shows the grain or subgrain size-distribution function, $f(x)$, for different milling times corresponding to the calculated m and σ values from the Eqs. 6 and 7. It can be seen that the size distribution is considerably narrowed with milling. However, after 40-h milling, further deformation does not have any significant effect on size distribution.

Annealing

The alloy powders milled for 80 h were annealed at 700, 800, and 900 °C for 1 h. Figure 9 shows the variations of average crystallite size after annealing. This figure indicates that the ultrafine grain structure in as-milled powder is retained even beyond 800 °C, while in matrix alloy without dispersoid begins to recrystallize about 700 °C. In other words, the addition of Y_2O_3 dispersoid increases the recrystallization temperature beyond 800 °C. Thermal studies on the ODS steels show that the Y_2O_3 particles which are dissolved during mechanical alloying [20, 21] mainly precipitate on the grain boundaries during heat

treating [6, 22, 23]. Hence, it appears that these precipitates can act as barriers to grain growth resulting in increased abnormal grain growth temperature. The similar result has been reported by West on 14YWT steel which indicates the recrystallization and grain growth are essentially suppressed up to 850 °C [6]. It is worth to note that the above mechanism along with the formation of high angle grains due to absorption of dislocations by the grain boundaries during annealing [24] can encourage the ultrafine grains at high temperatures. The details of the distribution of subgrain or grain size during annealing are given in Fig. 10. These data reveal that the annealing process leads to a remarkable enlargement of the range of subgrain-size distribution which becomes wider at higher annealing temperature. This can be attributed to rearrangement of dislocation and subgrain growth [25] induced by recovery at 700 and 800 °C, resulting in an initial increase of the average crystallite size in the nanometer range (Fig. 9), and recrystallization and grain growth at 900 °C leading to a bimodal structure as shown in Fig. 10. The effect of

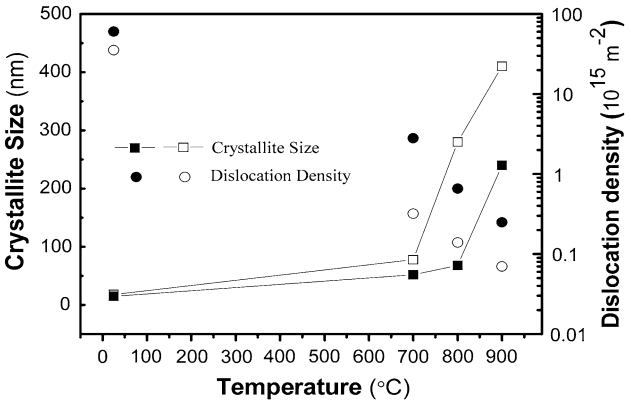

Fig. 9 Variations of average crystallite size and dislocation density with annealing temperature for the composite material (*solid*) and the matrix alloy (*open*)

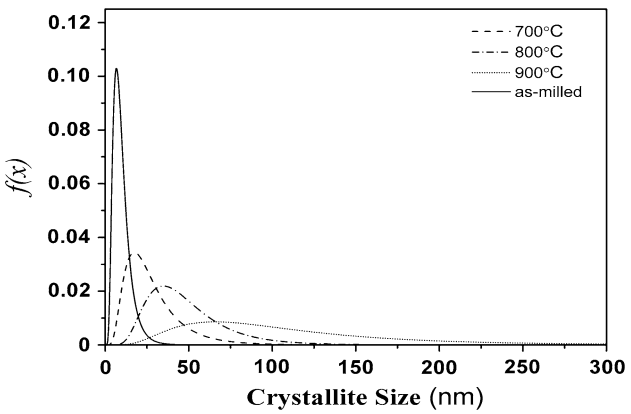

Fig. 10 The log-normal size distribution function, $f(x)$, for different annealing temperatures of ODS-steel

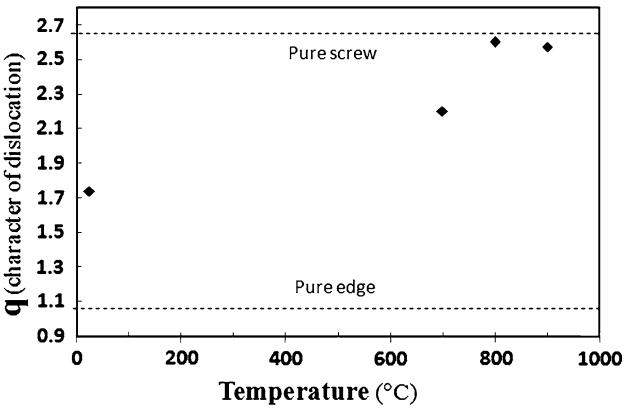

Fig. 11 The variation of character of dislocation during annealing

annealing temperature on the dislocation density is also shown in Fig. 9. As observed, the dislocation density decreases significantly with increasing temperature that corresponds to recovery in the alloy. It can be seen that the dislocations can annihilate more rapidly in the matrix alloy in comparison to the ODS alloy owing to oxide particle pinning mechanism. Since the climb mechanism occurs much more rapidly at high temperatures than at low temperatures due to an increase in vacancy motion, and the slip mechanism, however, has only a small dependence on temperature [25], the annihilation of dislocations is mainly caused by the thermally activated motion of edge components of dislocations. Hence, as can be seen in Fig. 11, with increasing temperature, the edge component of dislocation reduces.

Conclusion

The effects of milling time and post annealing temperature on the microstructural characteristics of ODS-steel and the unreinforced matrix were evaluated by X-ray diffraction line profile analysis based on the modified Williamson–Hall and the modified Warren–Averbach methods. The conclusions are summarized as follows:

1. The presence of nano-oxide particles in the ODS steel caused an initial sharp decrease in the average crystallite size; however, with increasing milling time, the crystallite size of the unreinforced alloy reached the comparable values of the reinforced material, which was about 20 nm after a milling time of 80 h.
2. At the initial milling stages, the average dislocation density increased at a significant rate, but it diminished at higher milling times. The rate of increase in the dislocation density was notably enhanced by the presence of nano-oxide particles in the reinforced steel.

3. The results of X-ray diffraction line profile analysis showed that the contribution of screw components to the total dislocation density was reduced with continued milling up to 40 h, owing to annihilation by cross slip. At higher milling times, the proportion of screw components showed a small increase, which can be attributed to the rearrangement of low angle grain boundaries into high angle grain boundaries.
4. The grain- or subgrain-size distribution was considerably narrowed with the milling up to 40 h, and further deformation did not show a notable effect on size distribution.
5. Annealing at 700 and 800 °C in ODS alloy resulted in an ultrafine grain structure consistent with that of as-milled powder, while in the matrix alloy, a bimodal structure was found about 700 °C due to recrystallization indicating the influence of oxide particles on retardation of recrystallization.

References

1. Oksiuta P, Olier P, Carlan Yde, Baluc N (2009) J Nucl Mater 393:114
2. Murty KL, Charit I (2008) J Nucl Mater 383:189
3. Hoffelner W (2010) J Mater Sci 45:2247. doi:10.1007/s10853-010-4236-7
4. Suryanarayana C (2001) Prog Mater Sci 46:1
5. Koch CC, Scattergood RO, Youssef KM, Chan E, Zhu YT (2010) J Mater Sci. doi:10.1007/s10853-010-4252-7
6. West MK (2006) Processing and characterization of oxide dispersion strengthened 14YWT ferritic alloys. PhD Thesis, University of Tennessee, Knoxville
7. Williamson GK, Hall WH (1953) Acta Metall 1:22
8. Warren BE, Averbach BL (1950) J Appl Phys 21:595
9. Ungar T, Borbely A (1996) Appl Phys Lett 69:3173
10. Ungar T, Victoria M, Marmy P, Hanak P, Szenes G (2000) J Nucl Mater 276:278
11. Movaghar Garabagh MR, Hossein Nedjad S, Nili Ahmadabadi M (2008) J Mater Sci 43:6840. doi:10.1007/s10853-008-2992-4
12. Schafler E, Zehetbauer M, Ungar T (2001) Mater Sci Eng A319–321:220
13. Ungar T, Gubicza J, Hanak P, Alexandrov I (2001) Mater Sci Eng A319–321:274
14. Ungar T (2001) Mater Sci Eng A309–310:14
15. Hinds WC (1999) Aerosol technology: properties, behavior and measurement of airbone particles. Wiley, New York
16. Langford JI, Wilson AJC (1978) J Appl Crystallogr 11:102
17. Fecht HJ (1995) Nanostruct Mater 6:33
18. Estrin Y, Toth LS, Molinari A, Brechet Y (1998) Acta Mater 46:5509
19. Zehetbauer M (1993) Acta Metall 41:589
20. Rahmanifard R, Farhangi H, Novinrooz AJ, Mater Sci Eng A (accepted)
21. Kimura Y, Takaki S, Suejima S, Uemori R, Tamehiro H (1999) ISIJ Int 39:176
22. Eislet ChCh, Klimenkov M, Lindau R, Moslang A, Sandim HRZ, Padilha AF, Raabe D (2009) J Nucl Mater 385:231
23. Eislet ChCh, Klimenkov M, Lindau R, Moslang A (2009) J Nucl Mater 386–388:525
24. Oksiuta Z, Boehm-Courjault E, Baluc N (2010) J Mater Sci 45:3921. doi:10.1007/s10853-010-4457-9
25. Humphreys FJ, Hatherly M (2004) Recrystallization and related annealing phenomena. Pergamon Elsevier, New York